PUBLISHED VERSION

http://hdl.handle.net/2440/56484

A full vectorial model for pulse propagation in emerging waveguides with subwavelength structures part II: Stimulated Raman Scattering

Mark D. Turner, Tanya M. Monro and Shahraam Afshar V.

Centre of Expertise in Photonics, School of Chemistry & Physics, The University of Adelaide, Adelaide, SA 5005, Australia.

shahraam.afshar@adelaide.edu.au

http://www.physics.adelaide.edu.au/photonics

Abstract: The significance of full vectorial pulse propagation through emerging waveguides has not been investigated. Here we report the development of a generalised vectorial model of nonlinear pulse propagation due to the effects of Stimulated Raman Scattering (SRS) in optical waveguides. Unlike standard models, this model does not use the weak guidance approximation, and thus accurately models the modal Raman gain of optical waveguides in the strong guidance regime. Here we develop a vectorial-based nonlinear Schrödinger Eq. (VNSE) to demonstrate how the standard model fails in certain regimes, with up to factors of 2.5 enhancement in Raman gain between the VNSE and the standard model. Using the VNSE we are able to explore opportunities for tailoring of the modal Raman gain spectrum to achieve effects such as gain flattening through design of the optical fiber.

References and links

1. S. Afshar V. and T. Monro, "A full vectorial model for pulse propagation in emerging waveguides with subwavelength structures part I: Kerr nonlinearity," Opt. Express **17**(4), 2298–2318 (2009).
2. M. Foster, A. Turner, M. Lipson, and A. Gaeta, "Nonlinear optics in photonic nanowires," Opt. Express **16**(2), 1300–1320 (2008).
3. M. Lamont, C. de Sterke, and B. Eggleton, "Dispersion engineering of highly nonlinear As_2S_3 waveguides for parametric gain and wavelength conversion," Opt. Express **15**(15), 9458–9463 (2007).
4. H. Ebendorff-Heidepriem, P. Petropoulos, S. Asimakis, V. Finazzi, R. Moore, K. Frampton, F. Koizumi, D. Richardson, and T. Monro, "Bismuth glass holey fibers with high nonlinearity," Opt. Express **12**(21), 5082–5087 (2004). URL http://www.opticsexpress.org/abstract.cfm?URI=oe-12-21-5082.
5. G. Renversez, B. Kuhlmey, and R. McPhedran, "Dispersion management with microstructured optical fibers: ultraflattened chromatic dispersion with low losses," Opt. Lett. **28**(12), 989–991 (2003). URL http://ol.osa.org/abstract.cfm?URI=ol-28-12-989.
6. A. Mussot, M. Beaugeois, M. Bouazaoui, and T. Sylvestre, "Tailoring CW supercontinuum generation in microstructured fibers with two-zero dispersion wavelengths," Opt. Express **15**(18), 11,553–11,563 (2007). URL http://www.opticsexpress.org/abstract.cfm?URI=oe-15-18-11553.
7. J. M. Dudley, G. Genty, and S. Coen, "Supercontinuum generation in photonic crystal fiber," Rev. Mod. Phys. **78**(4), 1135–1184 (2006).

8. S. Yiou, P. Delaye, A. Rouvie, J. Chinaud, R. Frey, G. Roosen, P. Viale, S. Février, P. Roy, J. Auguste and J. Blondy, "Stimulated Raman scattering in an ethanol core microstructured optical fiber," Opt. Express **13**(12), 4786–4791 (2005).

9. S. Atakaramians, S. Afshar V., B. Fischer, D. Abbott, and T. Monro, "Porous fibers: a novel approach to low loss THz waveguides," Opt. Express **16**(12), 8845–8854 (2008).

10. M. Foster and A. Gaeta, "Ultra-low threshold supercontinuum generation in sub-wavelength waveguides," Opt. Express **12**(14), 3137–3143 (2004). URL http://www.opticsexpress.org/abstract.cfm?URI=oe-12-14-3137.

11. Y. Lizé, E. Mägi, V. Ta'eed, J. Bolger, P. Steinvurzel, and B. Eggleton, "Microstructured optical fiber photonic wires with subwavelength core diameter," Opt. Express **12**(14), 3209–3217 (2004). URL http://www.opticsexpress.org/abstract.cfm?URI=oe-12-14-3209.

12. S. Afshar V., S. Warren-Smith, and T. Monro, "Enhancement of fluorescence-based sensing using microstructured optical fibres," Opt. Express **15**(26), 17,891–17,901 (2007).

13. M. Foster, J. Dudley, B. Kibler, Q. Cao, D. Lee, R. Trebino, and A. Gaeta, "Nonlinear pulse propagation and supercontinuum generation in photonic nanowires: experiment and simulation," Appl. Phys. B: Lasers and Optics **81**(2), 363–367 (2005).

14. Q. Xu, V. Almeida, R. Panepucci, and M. Lipson, "Experimental demonstration of guiding and confining light in nanometer-size low-refractive-index material," Opt. Lett. **29**(14), 1626–1628 (2004).

15. M. Foster, A. Turner, R. Salem, M. Lipson, and A. Gaeta, "Broad-band continuous-wave parametric wavelength conversion in silicon nanowaveguides," Opt. Express **15**(20), 12,949–12,958 (2007).

16. V. R. Almeida, Q. Xu, C. A. Barrios, and M. Lipson, "Guiding and confining light in void nanostructure," Opt. Lett. **29**(11), 1209–1211 (2004). URL http://ol.osa.org/abstract.cfm?URI=ol-29-11-1209.

17. M. Nagel, A. Marchewka, and H. Kurz, "Low-index discontinuity terahertz waveguides," Opt. Express **14**(21), 9944–9954 (2006).

18. H. Fukuda, K. Yamada, T. Shoji, M. Takahashi, T. Tsuchizawa, T. Watanabe, J. Takahashi, and S. Itabashi, "Four-wave mixing in silicon wire waveguides," Opt. Express **13**(12), 4629–4637 (2005).

19. G. Wiederhecker, C. Cordeiro, F. Couny, F. Benabid, S. Maier, J. Knight, C. Cruz, and H. Fragnito, "Field enhancement within an optical fibre with a subwavelength air core," Nature **1**(2), 115–118 (2007).

20. F. Benabid, J. C. Knight, G. Antonopoulos, and P. S. J. Russell, "Stimulated Raman scattering in hydrogen-filled hollow-core photonic crystal fiber," Science **298**(5592), 399–402 (2002). USA.

21. F. Benabid, G. Bouwmans, J. Knight, P. Russell, and F. Couny, "Ultrahigh Efficiency Laser Wavelength Conversion in a Gas-Filled Hollow Core Photonic Crystal Fiber by Pure Stimulated Rotational Raman Scattering in Molecular Hydrogen," Phys. Rev. Lett. **93**(12), 123,903 (2004).

22. S. Konorov, D. Sidorov-Biryukov, A. Zheltikov, I. Bugar, D. Chorvat Jr, D. Chorvat, V. Beloglazov, N. Skibina, M. Bloemer, and M. Scalora, "Self-phase modulation of submicrojoule femtosecond pulses in a hollow-core photonic-crystal fiber," Appl. Phys. Lett. **85**, 3690 (2004).

23. G. P. Agrawal, *Nonlinear Fiber Optics* (Academic Press, 2007).

24. C. Headley and G. P. Agrawal, "Unified description of ultrafast stimulated Raman scattering in optical fibers," J. Opt. Soc. Am. B **13**(10), 2170–2177 (1996).

25. J. Driscoll, X. Liu, S. Yasseri, I. Hsieh, J. Dadap, and R. Osgood, "Large longitudinal electric fields (E_z) in silicon nanowire waveguides," Opt. Express **17**(4), 2797–2804 (2009).

26. K. Thyagarajan and C. Kakkar, "Novel fiber design for flat gain Raman amplification using single pump and dispersion compensation in S band," J. Lightwave Technol. **22**(10), 2279–2286 (2004).

27. X. G. Chen, N. C. Panoiu, and R. M. Osgood, "Theory of Raman-mediated pulsed amplification in silicon-wire waveguides," IEEE J. Quantum Electron. **42**(1-2), 160–170 (2006).

28. J. I. Dadap, N. C. Panoiu, X. G. Chen, I. W. Hsieh, X. P. Liu, C. Y. Chou, E. Dulkeith, S. J. McNab, F. N. Xia, W. M. J. Green, L. Sekaric, Y. A. Vlasov, and R. M. Osgood, "Nonlinear-optical phase modification in dispersion-engineered Si photonic wires," Opt. Express **16**(2), 1280–1299 (2008).

29. K. Okamoto, *Fundamentals of Optical Waveguides* (Academic Press, 2006).

30. B. Kuhlmey, T. White, G. Renversez, D. Maystre, L. Botten, C. de Sterke, and R. McPhedran, "Multipole method for microstructured optical fibers. II. Implementation and results," J. Opt. Soc. Am. B **19**(10), 2331–2340 (2002).

31. T. White, B. Kuhlmey, R. McPhedran, D. Maystre, G. Renversez, C. de Sterke, and L. Botten, "Multipole method for microstructured optical fibers. I. Formulation," J. Opt. Soc. Am. B **19**(10), 2322–2330 (2002).

32. A. Snyder and J. Love, *Optical waveguide theory* (Kluwer Academic Pub, 1983).

33. A. Kireev and T. Graf, "Vector coupled-mode theory of dielectric waveguides," IEEE J. Quantum Electron. **39**(7), 866–873 (2003).

34. P. Butcher and D. Cotter, *The Elements of Nonlinear Optics* (Cambridge University Press, 1990).

35. Q. Lin, O. J. Painter, and G. P. Agrawal, "Nonlinear optical phenomena in silicon waveguides: Modeling and applications," Opt. Express **15**(25), 16,604–16,644 (2007).

36. R. Hellwarth, "Third-order optical susceptibilities of liquids and solids," Prog. Quantum Electron. **5**(1), 2–68 (1977).

37. A. Efimov, A. Taylor, F. Omenetto, J. Knight, W. Wadsworth, and P. Russell, "Phase-matched third harmonic generation in microstructured fibers," Opt. Express **11**(20), 2567–2576 (2003).

38. D. Dimitropoulos, V. Raghunathan, R. Claps, and B. Jalali, "Phase-matching and Nonlinear Optical Processes in Silicon Waveguides," Opt. Express **12**(1), 149–160 (2004).
39. V. Ta'eed, N. Baker, L. Fu, K. Finsterbusch, M. Lamont, D. Moss, H. Nguyen, B. Eggleton, D. Choi, S. Madden and B. Luther-Davies, "Ultrafast all-optical chalcogenide glass photonic circuits," Opt. Express **15**(15), 9205–9221 (2007).
40. R. Slusher, G. Lenz, J. Hodelin, J. Sanghera, L. Shaw, and I. Aggarwal, "Large Raman gain and nonlinear phase shifts in high-purity As 2 Se 3 chalcogenide fibers," J. Opt. Soc. Am. B **21**(6), 1146–1155 (2004).
41. V. E. Perlin and H. G. Winful, "Optimal design of flat-gain wide-band fiber Raman amplifiers," J. Lightwave Technol. **20**(2), 250–254 (2002).
42. S. Cui, J. S. Liu, and X. M. Ma, "A novel efficient optimal design method for gain-flattened multiwavelength pumped fiber Raman amplifier," IEEE Photon. Technol. Lett. **16**(11), 2451–2453 (2004).
43. C. Kakkar and K. Thyagarajan, "High gain Raman amplifier with inherent gain flattening and dispersion compensation," Opt. Commun. **250**(1-3), 77–83 (2005).
44. R. Jose and Y. Ohishi, "Higher nonlinear indices, Raman gain coefficients, and bandwidths in the TeO/sub 2/-ZnO-Nb/sub 2/O/sub 5/-MoO/sub 3/ quaternary glass system," Appl. Phys. Lett. **90**(21), 211,104–1–211,104–211,104–3 (2007). USA.
45. R. Stegeman, L. Jankovic, K. Hongki, C. Rivero, G. Stegeman, K. Richardson, P. Delfyett, G. Yu, A. Schulte, and T. Cardinal, "Tellurite glasses with peak absolute Raman gain coefficients up to 30 times that of fused silica," Opt. Lett. **28**(13), 1126–1128 (2003). USA.
46. Q. Guanshi, R. Jose, and Y. Ohishi, "Design of ultimate gain-flattened O+ E and S+ C+ L ultrabroadband fiber amplifiers using a new fiber Raman gain medium," J. Lightwave Technol. **25**(9), 2727–2738 (2007). USA.
47. A. Mori, H. Masuda, K. Shikano, and M. Shimizu, "Ultra-wide-band tellurite-based fiber Raman amplifier," J. Lightwave Technol. **21**(5), 1300–1306 (2003). USA.

1. Introduction

Recently, the growing interest in optical waveguides with high nonlinearity [1-4] and specific dispersion characteristics [5-8] has led to the development of emerging waveguides [1] that contain inhomogeneous and complex transverse structure [8, 9], subwavelength inclusions (or holes) [9-11] and high refractive index contrast. These emerging waveguides often operate in regimes of strong guidance where light within the waveguide is tightly confined and thus weak guidance approximation is no longer valid.

Due to the tight confinement these strongly guiding optical waveguides often possess extreme nonlinearity, dispersion and other optical characteristics not possible in standard optical waveguides. For example, optical waveguides containing subwavelength features with high refractive index contrast have been shown to have significant discontinuities in the modal field distributions at the boundary between two dielectric materials [9, 12-19]. This arises from Maxwell's continuity Eqs. that state across a dielectric boundary in the absence of sources, the normal component of the electric displacement field vector is continuous [19]. Hence the normal component of the electric field vector has a discontinuity proportional to the ratio of the dielectric constants of the two media. This creates a high intensity layer at the low refractive index side of the interface [19].

Another feature of emerging waveguides is the use of inhomogeneous and complex structure within optical waveguides, which provides great flexibility for tailoring the optical characteristics of the waveguide. One example is a microstructured optical fiber (MOF) which can have any arbitrary fiber cross section giving the ability to tailor the nonlinearity, dispersion, absorption etc. One post processing technique availiable to MOFs containing holey structure is filling with gases and liquids to further engineer the optical characteristics of the fiber [8, 20-22]. For example enhancement of stimulated Raman scattering by filling the core of a MOF with the nonlinear liquid ethanol [8], filling photonic crystal fibers with Hydrogen gas to produce Raman effects at low power thresholds [20, 21] or with helium gas to decrease the effects of self-phase modulation [22].

These features of emerging waveguides offer great potential for nonlinear optical devices. However, due to their assumptions of weak guidance, standard pulse propagation models of the

effects of dispersion and nonlinearity are not valid in this regime of strong guidance. Hence there is a need for new formulations of nonlinear effects to accurately model nonlinear pulse propagation within these emerging waveguides.

The standard model for nonlinear effects in optical fibers such as Stimulated Raman Scattering (SRS) has been developed extensively [23, 24]. Experimental investigations within weakly guiding optical fibers agree with these standard models [23]. In this standard model (SM) of Raman effects in optical waveguides, the Raman gain is given by [23]:

$$g(m^{-1}W^{-1}) = \frac{g_R}{A_{eff}}, \tag{1}$$

where g_R is the bulk Raman gain coefficient of the host material measured in metres per watt, and A_{eff} is the effective area measured in m^2. The standard model (SM) is based upon the weak guidance approximation which assumes the fields are purely transverse and it neglects the spatial dependence of both the refractive index and bulk Raman gain coefficient. The SM also assumes no differences in the modal field distributions of the pump and Stokes fields. These approximations are only valid for optical fibers in the weak guidance regime, where the core size is large and the refractive index contrast is small. It has been shown that in the regime of subwavelength features with high refractive index contrast, the fields can have significant longitudinal components of the electric field vector and thus the mode can no longer can be considered as purely transverse, which can have significant impact on Kerr nonlinearity [1, 25]. An alteration to the SM was used in [26] to numerically calculate modal Raman gain spectra. This altered model takes into account the spatial dependence of the bulk Raman gain coefficient, as well as the differences in the pump and Stokes fields which can differ significantly over the Raman spectrum within strongly guiding optical waveguides. Here we shall call this model the altered standard model (ASM). However, both the ASM and SM only consider the scalar form of the fields and thus are only valid in the regime of weak guidance.

There have been attempts to create rigorous vectorial nonlinear models for silicon waveguides [27, 28] that include dispersion, Raman effects, two photon absorption and free carrier effects, which all have significance in silicon waveguides. Note that the models developed in [27, 28] only consider the linear and nonlinear interactions between two specified eigenmodes of the optical waveguide. However, a rigorous model must use a complete basis set of modes to fully describe the pulse propagation. Even in the case of a single mode optical fiber, there are two different polarisations to consider.

In [25, 27] it is mentioned that the longitudinal components of the electric field could affect the nonlinearity of the waveguide. However, in the numerical analysis in [27], the E_z fields contributes less than 1% of the total vector field amplitude, such that the effect of E_z on nonlinearity can be ignored. Whilst [25] investigates in which regimes the E_z fields become significant, the impact of E_z on nonlinear effects such as SRS is not discussed. Thus to the best of our knowledge, there has been no investigation into effects of the longitudinal component of the electric field to SRS.

This paper has two main purposes. Firstly, we develop a complete vectorial model for pulse propagation under the effects of SRS and dispersion within an arbitrary optical waveguide. Secondly, we investigate the effects of the longitudinal components of electromagnetic fields on Raman gain within emerging waveguides.

Here we develop a vectorially-based nonlinear Schrödinger Eq. (VNSE), for SRS in optical waveguides. The VNSE is derived from Maxwell's Eqs. that are in their full vectorial form within the context of optical waveguides that possess the single constraint of translational invariance. The VNSE is able to accurately predict the modal Raman gain of an optical waveguide in both the weakly guiding and strongly guiding regimes.

The VNSE simultaneously considers the set of eigenmodes of the optical waveguide, and

their nonlinear interactions, which leads to new terms in the pulse propagation model not shown before in [23, 27, 28]. However, for simplicity here we only consider just SRS and dispersion. The models in [23, 27, 28] consider other important phenomena such as free carrier effects and two photon absorption. Our approach for deriving the VNSE for SRS here and Kerr nonlinearity in [1] could be used to model these other effects as well. However, this is not within the scope of this paper.

Based on the developed VNSE, we investigate the impact of E_z on SRS, and show that it can effect the calculations for the modal Raman gain, especially in the regime of high index and subwavelength structured waveguides.

In Section 2 we build on the development of a VNSE for Kerr nonlinearity in [1] and now consider the effects of SRS. We explicitly derive the modal Raman gain in terms of the refractive index and bulk Raman gain coefficient of the glass, liquid, gas or other materials within the waveguide. In Section 3 we numerically calculate the modal Raman gain using the VNSE and SM and observe large differences in these regimes of strong guidance. In Section 4 we investigate using the VNSE for tailoring of the modal Raman gain of an optical waveguide through the design of the waveguide itself and significant alteration to the shape of the Raman gain spectrum is observed leading to possible effects such as gain flattening.

2. Development of VNSE

To develop a vectorial based nonlinear Schr$\ddot{o}$dinger Eq. we use perturbation theory. We define the unperturbed fields in terms of a particular eigenmode of the waveguide without dispersion and nonlinearity and then form the perturbed fields as a linear superposition of the basis set of unperturbed eigenmodes. The unperturbed system is defined by two independent sets of Maxwell's Eqs. for the pump and Stokes fields, which in the absense of sources are:

$$\nabla \times \tilde{\mathbf{E}}_{o\kappa}(\mathbf{r}, \omega) = i\mu_0 \omega \tilde{\mathbf{H}}_{o\kappa}(\mathbf{r}, \omega), \tag{2}$$

$$\nabla \times \tilde{\mathbf{H}}_{o\kappa}(\mathbf{r}, \omega) = -i\omega \left[\varepsilon_0 \tilde{\mathbf{E}}_{o\kappa}(\mathbf{r}, \omega) + \tilde{\mathbf{P}}_\kappa^L(\mathbf{r}, \omega) \right], \tag{3}$$

where $\kappa = p, s$ denoting the pump and Stokes and the unperturbed fields are at two different frequencies ω_p and ω_s. The tilde above the fields represents performed done in the Fourier domain. The Fourier transform is defined as:

$$F(\mathbf{r}, t) = \frac{1}{2\pi} \int_{-\infty}^{\infty} \tilde{F}(\mathbf{r}, \omega) e^{-i\omega t} d\omega. \tag{4}$$

The linear polarisation of the optical waveguide is defined as:

$$\tilde{\mathbf{P}}_\kappa^L(\mathbf{r}, \omega) = \varepsilon_0 \chi^{(1)}(-\omega; \omega) \cdot \tilde{\mathbf{E}}_{o\kappa}, \tag{5}$$

where for an isotropic medium the linear susceptibility can be related to the refractive index:

$$n^2(\mathbf{r}, \omega) = 1 + \chi^{(1)}(-\omega; \omega). \tag{6}$$

The two differential Eqs. (2) and (3) can be solved to obtain a set of full vectorial eigenmodes of the unperturbed system. This set of both bound and leaky modes, in both the core and cladding of the optical waveguide, forms a complete set, such that any other electromagnetic field can be written as a superposition of these modes.

In practice these eigenmodes can be obtained numerically using the Finite Element method [29], the Multipole Method [30, 31], etc. These numerical calculations are based entirely on the linear refractive index geometry of the waveguide.

To derive a full vectorial nonlinear pulse propagation Eq. that describes the evolution of a particular mode under the effects of dispersion and nonlinear SRS, we define the unperturbed fields as a single eigenmode of the optical waveguide i.e. the μth eigenmode with the form [32]:

$$\tilde{\mathbf{E}}_{o\kappa} = \frac{1}{2}\mathbf{E}_{\kappa\mu}\delta(\omega - \omega_{\kappa}), \tag{7}$$

$$\tilde{\mathbf{H}}_{o\kappa} = \frac{1}{2}\mathbf{H}_{\kappa\mu}\delta(\omega - \omega_{\kappa}), \tag{8}$$

$$\mathbf{E}_{\kappa\mu} = \frac{\mathbf{e}_{\kappa\mu}(x,y)e^{i\beta_{\kappa\mu}z}}{\sqrt{N_{\kappa\mu}}} + c.c., \qquad \mathbf{H}_{\kappa\mu} = \frac{\mathbf{h}_{\kappa\mu}(x,y)e^{i\beta_{\kappa\mu}z}}{\sqrt{N_{\kappa\mu}}} + c.c., \tag{9}$$

where $\beta_{p\mu}$ and $\beta_{s\mu}$ are the propagation constants for the μth mode of the unperturbed eigenmodes of the pump and Stokes fields and c.c. is the complex conjugate which we shall leave out from here for simplicity. The eigenmodes of the optical waveguide form an orthonormal basis set:

$$\frac{1}{2}\int(\mathbf{e}_{\kappa\mu}^{*} \times \mathbf{h}_{\kappa\eta}) \cdot \hat{z}dA = N_{\kappa\mu\eta}\delta_{\mu\eta} = N_{\kappa\mu}, \qquad N_{\kappa\mu} = \frac{1}{2}\int(\mathbf{e}_{\kappa\mu}^{*} \times \mathbf{h}_{\kappa\mu}) \cdot \hat{z}dA. \tag{10}$$

Similarly we define the perturbed system through Maxwell's Eqs. (which now include both nonlinearity and dispersion) by considering two quasi-monochromatic electric and magnetic fields $\mathbf{E}_{\kappa}$ and $\mathbf{H}_{\kappa}$. Unlike previous models that consider just the interaction between two modes of the optical waveguide [23, 27, 28], here we wish to have a complete model that includes all modes of the waveguide, which requires the use of a basis set of eigenmodes:

$$\tilde{\mathbf{E}}_{\kappa} = \frac{1}{2}\sum_{\eta}\tilde{a}_{\kappa\eta}(z,\omega - \omega_{\kappa})\mathbf{E}_{\kappa\eta}, \tag{11}$$

$$\tilde{\mathbf{H}}_{\kappa} = \frac{1}{2}\sum_{\eta}\tilde{a}_{\kappa\eta}(z,\omega - \omega_{\kappa})\mathbf{H}_{\kappa\eta}. \tag{12}$$

By using a complete basis set of modes including the discrete set of bound and leaky both forward and backward propagating, we have a more complete description of the pulse propagation than using a single mode. Even in the case of a single mode optical waveguide there may be situations where interactions between bound and leaky modes are significant. However, here we do not include the continuous set of radiation modes, as these modes typically contain information of fields far from the core of the optical waveguide [32]. Also, implementing this extra information into the basis set increases the complexity of the required numerical calculations. It should also be pointed out that we have not used the vector coupled-mode formalism developed in [33], as here we consider the modes to be the solutions of the entire system, where in [33] an array of individual waveguides each with their own set of modes is considered.

In time domain, the coefficients $a_{\kappa\eta}(z,t)$ are the modal amplitudes and $\left|a_{\kappa\eta}(z,t)\right|^2$ is the pulse power envelope for the ηth (pump/Stokes) mode. Physically these modal amplitudes describe how the modes of the optical fiber evolve as they propagate along the waveguide with the effects of both dispersion and nonlinearity where $\left|a_{\kappa\eta}(0,t)\right|^2$ is the initial pulse of the ηth mode at the start of the waveguide.

We shall assume here that since each of Maxwell's Eqs. contain electric, magnetic and polarisation fields oscillating at either ω_p or ω_s, the perturbed Maxwell's Eqs. can still be separated into two sets, one each for the pump and Stokes fields:

$$\nabla \times \tilde{\mathbf{E}}_\kappa = \frac{i\mu_0\omega}{2}\sum_\eta \tilde{a}_{\kappa\eta}\mathbf{H}_{\kappa m,} \tag{13}$$

$$\nabla \times \tilde{\mathbf{H}}_\kappa = \frac{-i\omega\varepsilon_0 n^2(\mathbf{r},\omega)}{2}\sum_\eta \tilde{a}_{\kappa\eta}\mathbf{E}_{\kappa\eta} - i\omega\tilde{\mathbf{P}}_\kappa^{NL}, \tag{14}$$

This is valid as long as the two quasi-monochromatic pump and Stokes pulses do not spectrally overlap. Having now explicitly defined Maxwell's Eqs. and the fields for the unperturbed and perturbed systems, we now derive a pulse propagation Eq. of a particular mode propagating under the effects of dispersion and nonlinearity. The SM is derived using the wave Eq., which makes the assumption that $\nabla \cdot \mathbf{E} = 0$, by assuming that the permitivity of the optical waveguide has negligible spatial dependence. We do not use this technique since we are interested in waveguides that in general have permittivities with strong spatial dependence such as a MOF containing an array of subwavelength holes. Instead here we shall use the Reciprocal theorem [32], as used in [1, 27], using the unperturbed and perturbed Stokes fields:

$$\frac{\partial}{\partial z}\int \mathbf{F}_{cs}\cdot\hat{z}dA = \int \nabla\cdot\mathbf{F}_{cs}dA, \tag{15}$$

where the vector field $\mathbf{F}_{cs}$ is given by:

$$\mathbf{F}_{cs} = \tilde{\mathbf{E}}_{os}^* \times \tilde{\mathbf{H}}_s + \tilde{\mathbf{E}}_s \times \tilde{\mathbf{H}}_{os}^*. \tag{16}$$

Eq. (15), will allow us to relate the unperturbed fields to the perturbed fields and create a propagation Eq. for Stokes pulses under dispersion and nonlinear effects such as SRS. The right hand side of Eq. (15), can be expanded using Eqs. (2), (3), (13), (14), Maxwell's Eqs. for the unperturbed and perturbed system. A Taylor series expansion on $\omega n^2(\mathbf{r},\omega) = \omega_s n^2(\mathbf{r},\omega_s) + \Delta\omega_s\left[\frac{\partial}{\partial\omega}\left(\omega n^2(\mathbf{r},\omega)\right)\right]_{\omega=\omega_s} + O(\Delta\omega_s^2)$ is used to separate dispersion into the order of $\Delta\omega_s = \omega - \omega_s$. We then apply Eq. (10), the orthonormality condition to the left hand side of Eq. (15) and arrive with Eq. (17), which is the general nonlinear pulse propagation Eq.

$$\begin{aligned}
\frac{\partial\tilde{a}_{s\mu}(z,\omega-\omega_s)}{\partial z} &= i\Delta\omega_s\beta_{s\mu}^1\tilde{a}_{s\mu}(z,\omega-\omega_s) + i\Delta\omega_s\sum_{\eta\neq\mu}\beta_{s\eta}^1\tilde{a}_{s\eta}(z,\omega-\omega_s) + O(\Delta\omega_s^2) \\
&+ \frac{i}{2}\int\mathbf{E}_{s\mu}^*\cdot\omega\tilde{\mathbf{P}}_s^{NL}(\mathbf{r},\omega)dA
\end{aligned} \tag{17}$$

where

$$\beta_{s\mu}^1 = \frac{1}{4N_{s\mu}}\int\left[\mu_0\left|\mathbf{h}_{s\mu}\right|^2 + \varepsilon_0\left[\frac{\partial}{\partial\omega}\left(\omega n^2(\mathbf{r},\omega)\right)\right]\big|_{\omega=\omega_s}\left|\mathbf{e}_{s\mu}\right|^2\right]dA \tag{18}$$

$$\beta_{s\eta}^1 = \frac{e^{i(\beta_{s\eta}-\beta_{s\mu})z}}{4\sqrt{N_{s\eta}N_{s\mu}}}\int\left[\mu_0\mathbf{h}_{s\eta}\cdot\mathbf{h}_{s\mu}^* + \varepsilon_0\left[\frac{\partial}{\partial\omega}\left(\omega n^2(\mathbf{r},\omega)\right)\right]\big|_{\omega=\omega_s}\mathbf{e}_{s\eta}\cdot\mathbf{e}_{s\mu}^*\right]dA \tag{19}$$

Eq. (17) is general and is of the same form as in [27]. However, here we consider a basis set of modes for the perturbed fields, which leads to a series of interactions in the pulse propagation model in both dispersion and nonlinearity.

In a single mode step index optical fiber, there are two bound modes corresponding to the two polarisations of the fundamental mode. The rest of the modes of the optical waveguide contribute to the set of Radiation modes that attenuate rapidly along the waveguide. These two bound modes can potentially interact with each other through dispersion and nonlinearity and thus it is important to consider the sum of interactions in Eq. (17), even within single mode step index fibers.

We shall now explicitly derive the expressions for the modal Raman gain and discuss their differences from standard definitions [23]. In the time domain, this general nonlinear pulse propagation Eq. has the form:

$$\frac{\partial a_{s\mu}(z,t)}{\partial z} = \hat{D} a_{s\mu}(z,t) - e^{i\omega_s t} \frac{\partial}{\partial t} \frac{e^{-i\beta_{s\mu} z}}{2\sqrt{N_{s\mu}}} \int \mathbf{e}_{s\mu}^* \bullet \mathbf{P}_s^{NL}(\mathbf{r},t) dA \qquad (20)$$

$$\hat{D} = i\beta_{s\mu}^1 \frac{\partial}{\partial t} + i \sum_{\eta \neq \mu} \beta_{s\eta}^1 \frac{\partial}{\partial t} + O(\frac{\partial^2}{\partial t^2}),$$

To derive the nonlinear Raman polarisation, we use the formalism in [34] for describing the nonlinear polarisation due to stimulated Raman scattering (SRS). The nonlinear Stokes polarisation can be split into its fast and slow time varying components:

$$\mathbf{P}_s^{NL}(\mathbf{r},t) = \frac{1}{2} \mathbf{P}_{\omega_s}(\mathbf{r},t) e^{-i\omega_s t} + c.c.,$$

where $\mathbf{P}_{\omega_s}(\mathbf{r},t)$ is given by the convolution of the Electric fields with the 3rd order nonlinear response function $\Phi^{(3)}_{-\omega_s;\omega_p,-\omega_p,\omega_s}$ [34].

$$\mathbf{P}_{\omega_s}^{(3)}(t) = \frac{3\varepsilon_0}{2} \int \int \int \mathbf{R}^{(3)}(\mathbf{r},t-t_1,t-t_2,t-t_3) \vdots \mathbf{E}_{\omega_p}(\mathbf{r},t_1) \mathbf{E}_{\omega_p}^*(\mathbf{r},t_2) \mathbf{E}_{\omega_s}(\mathbf{r},t_3)$$
$$\exp(i \sum_{r=1}^{3} \omega_r(t-t_r)) dt_1 dt_2 dt_3, \qquad (21)$$

where $\mathbf{E}_{-\omega'} = \mathbf{E}_{\omega'}^*$, $\omega_{1,2,3} = \omega_{p,-p,s}$ and $\mathbf{R}^{(3)}$ is the rank-4 Raman response tensor that is defined as [23, 35]:

$$\mathbf{R}^{(3)}(t-t_1,t-t_2,t-t_3) = \mathbf{R}(x,y,t-t_2)\delta(t-t_1)\delta(t_2-t_3). \qquad (22)$$

It is important to note that the spatial dependence of the Raman response tensor for waveguides must not be ignored in the case of optical waveguides containing complex cross-sectional geometry. Using Eq. (22) in Eq. (21) and expanding the electric field vectors using the time domain form of Eqs. (11), (12) the nonlinear Stokes polarisation becomes:

$$\mathbf{P}_{\omega_s}^{(3)}(t) = \frac{3\varepsilon_0}{2} \sum_{\eta,\sigma,\xi} \frac{e^{i(\beta_{p\eta}-\beta_{p\sigma}+\beta_{s\xi})}}{\sqrt{N_{p\eta}N_{p\sigma}N_{s\xi}}} a_{p\eta}(z,t)$$
$$\times \int \mathbf{R}(x,y,t-t_2) \vdots \mathbf{e}_{p\eta} \mathbf{e}_{p\sigma}^* \mathbf{e}_{s\xi} a_{p\sigma}^*(z,t_2) a_{s\xi}(z,t_2)$$
$$\times \exp(-i\Delta\omega(t-t_2)) dt_2, \qquad (23)$$

where $\Delta\omega = \omega_p - \omega_s$. Using Eq. (23) in Eq. (20) we arrive at the SRS pulse propagation Eq.:

$$
\begin{aligned}
\frac{\partial a_{s\mu}(z,t)}{\partial z} &= \hat{D}a_{s\mu}(z,t) + i\omega_s\left(1 + \frac{i}{\omega_s}\frac{\partial}{\partial t}\right)\frac{e^{-i\beta_{s\mu}z}}{4\sqrt{N_{s\mu}}}\int \mathbf{e}_{s\mu}^* \cdot \mathbf{P}_{-\omega_s}^{(3)}(t)dA \\
&= \hat{D}a_{s\mu}(z,t) + i\frac{3\varepsilon_0\omega_s}{8}\left(1 + \frac{i}{\omega_s}\frac{\partial}{\partial t}\right)\sum_{\eta,\sigma,\xi}\frac{e^{i(\beta_{p\eta}-\beta_{p\sigma}+\beta_{s\xi}-i\beta_{s\mu}z)}}{\sqrt{N_{p\eta}N_{p\sigma}N_{s\xi}N_{s\mu}}}a_{p\eta}(z,t) \\
&\quad \int \mathbf{e}_{s\mu}^* \cdot \int \mathbf{R}(x,y,t-t_2)\vdots\mathbf{e}_{p\eta}\mathbf{e}_{p\sigma}^*\mathbf{e}_{s\xi}a_{p\sigma}^*(z,t_2)a_{s\xi}(z,t_2) \\
&\quad \exp(-i\Delta\omega(t-t_2))dt_2 dA.
\end{aligned}
\tag{24}
$$

Eq. (24) is general and can be used for both short and long pulses, and for an arbitrary optical waveguide structure. Before we continue this analysis of SRS, we discuss another use for Eq. (24). In [1], Kerr nonlinearity was assumed to be instantaneous, i.e. the nonlinear response function had the form $R(x,y,t) = \chi_{ijkl}^{(3)}(x,y)\delta(t)$. This implies that there is no dispersion in the nonlinear coefficient n_2.

However, for ultrashort pulses with large bandwidth, a finite response function $k(x,y,t)$ may need to be considered for Kerr nonlinearity. If one lets $p = s$ in Eq. (24) and $R(x,y,t) = \chi_{ijkl}^{(3)}(x,y)k(x,y,t)$, one will have a VNSE for Kerr nonlinerity that now considers the dispersion of Kerr nonlinearity. This is beyond the scope of this paper, and would be a subject for future study.

For silica glass, the Raman response function as defined by Eq. (25):

$$
\mathbf{R}(x,y,\tau) = \frac{\chi_{xxxx}^{(3)}}{2}\left(f_a h_a(\tau)\delta_{ij}\delta_{kl} + \frac{1}{2}f_b h_b(\tau)\left(\delta_{ik}\delta_{jl} + \delta_{il}\delta_{jk}\right)\right),
\tag{25}
$$

where $i,j,k,l = x,y,z$. Eq. (25) has two components corresponding to the isotropic and anisotropic contributions to SRS [23, 36] which are denoted by a and b respectively. However due to the amorphous nature of glasses such as silica the isotropic contribution to SRS dominates throughout most of the Raman spectrum as discussed in [23, 36]. We include the anisotropic component for completeness.

We now specialise the pulse propagation Eq. to MOFs that contain amorphous materials such as silica glass, or liquids and gases. We assume that all materials within the optical fiber have the same form of the Raman reponse as shown in Eq. (25). If this is not valid, the more general Eq. (24) must be used. The 3rd order susceptibility tensor component, $\chi_{xxxx}^{(3)}$ is given by [23]:

$$
\chi_{xxxx}^{(3)}(x,y) = \frac{4\varepsilon_0 cn^2(x,y)n_2(x,y)}{3}
\tag{26}
$$

Again noting that here we consider the spatial dependence of $n^2(x,y)$, $n_2(x,y)$, $f_{a,b}(x,y)$ and $h_{a,b}(x,y,\tau)$, which from here on we shall assume implicitly. Using Eqs. (25), (26) in (24) we find the general nonlinear pulse propagation due to dispersion and SRS for silica glass becomes:

$$\frac{\partial a_{s\mu}(z,t)}{\partial z} = \hat{D}a_{s\mu}(z,t) + i\frac{\varepsilon_0^2 c\omega_s}{4}\left(1+\frac{i}{\omega_s}\frac{\partial}{\partial t}\right)\sum_{\eta,\sigma,\xi}\frac{e^{i(\beta_{p\eta}-\beta_{p\sigma}+\beta_{s\xi}-i\beta_{s\mu}z)}}{\sqrt{N_{p\eta}N_{p\sigma}N_{s\xi}N_{s\mu}}}a_{p\eta}(z,t)$$

$$\times \int f_a n^2 n_2 \left(\mathbf{e}_{s\mu}^* \cdot \mathbf{e}_{p\eta}\right)\left(\mathbf{e}_{p\sigma}^* \cdot \mathbf{e}_{s\xi}\right)$$

$$\times \int h_a(t-t_2)a_{p\sigma}^*(z,t_2)a_{s\xi}(z,t_2)\exp(-i\Delta\omega(t-t_2))dt_2$$

$$+ \frac{1}{2}f_b n^2 n_2 \left\{\left(\mathbf{e}_{p\sigma}^*\cdot\mathbf{e}_{p\eta}\right)\left(\mathbf{e}_{s\mu}^*\cdot\mathbf{e}_{s\xi}\right)+\left(\mathbf{e}_{s\mu}^*\cdot\mathbf{e}_{p\sigma}^*\right)\left(\mathbf{e}_{p\eta}\cdot\mathbf{e}_{s\xi}\right)\right\}$$

$$\times \int h_b(t-t_2)a_{p\sigma}^*(z,t_2)a_{s\xi}(z,t_2)\exp(-i\Delta\omega(t-t_2))dt_2 dA. \qquad (27)$$

Eq. (27) is a general pulse propagation Eq. for dispersion and SRS within optical fibers provided that the materials have the Raman response form given by Eq. (22). Eq. (27) does not use the adiabatic approximation and thus can be used for ultrashort pulses. Due to the full vectorial formulation as well as the use of a basis set of modes, the form of Eq. (27) is now different to that in [23].

If we now assume that the pump and Stokes pulses are much longer than the Raman response time, we can make the adiabatic approximation and bring the pulse amplitudes outside the convolution integral:

$$\int h_{a,b}(t-t_2)a_{p\sigma}^*(t_2)a_{s\xi}(t_2)\exp(-i\Delta\omega(t-t_2))dt_2 = a_{p\sigma}^* a_{s\xi}\tilde{h}_{a,b}(-\Delta\omega),$$

From here on we shall only consider the imaginary part of $\tilde{h}_{a,b}(\Delta\omega)$ which leads to Raman gain, whereas the real component leads to Raman-induced refractive index changes [23]. The effect of such index changes on the pulse propagation is ignored here for simplicity. Also, note that $Im\left[\tilde{h}_{a,b}(\Delta\omega)\right]$ is an odd function i.e. $Im(\tilde{h}_{a,b}(-\Delta\omega)) = -Im(\tilde{h}_{a,b}(\Delta\omega))$ [23]. We now use the definition of the bulk Raman coefficient measured in mW^{-1} [23]:

$$g_{a,b}(x,y,\Delta\omega) = \frac{2f_{a,b}n_2\omega_s Im(\tilde{h}_{a,b}(\Delta\omega))}{c}.$$

where $\Delta\omega = \omega_p - \omega_s$. This leads to the following adiabatic pulse propagation Eq. for SRS:

$$\frac{\partial a_{s\mu}(z,t)}{\partial z} = \hat{D}a_{s\mu} + \frac{\varepsilon_0^2 c^2}{8}\left(1+\frac{i}{\omega_s}\frac{\partial}{\partial t}\right)\sum_{\eta,\sigma,\xi}\frac{e^{i(\beta_{p\eta}-\beta_{p\sigma}+\beta_{s\xi}-i\beta_{s\mu}z)}}{\sqrt{N_{p\eta}N_{p\sigma}N_{s\xi}N_{s\mu}}}a_{p\eta}a_{p\sigma}^* a_{s\xi}$$

$$\int g_a n^2\left(\mathbf{e}_{s\mu}^*\cdot\mathbf{e}_{p\eta}\right)\left(\mathbf{e}_{p\sigma}^*\cdot\mathbf{e}_{s\xi}\right)$$

$$+ \frac{1}{2}g_b n^2\left[\left(\mathbf{e}_{p\sigma}^*\cdot\mathbf{e}_{p\eta}\right)\left(\mathbf{e}_{s\mu}^*\cdot\mathbf{e}_{s\xi}\right)+\left(\mathbf{e}_{s\mu}^*\cdot\mathbf{e}_{p\sigma}^*\right)\left(\mathbf{e}_{p\eta}\cdot\mathbf{e}_{s\xi}\right)\right]dA \qquad (28)$$

The VNSE for SRS within MOFs as defined by Eq. (28) is rather different to that in [23]. Here we have considered the spatial dependence of the refractive index profile and bulk Raman gain coefficient, the vectorial form of the fields, the difference in the pump and Stokes fields and the possibility of interactions between the basis set of modes. It is important to note that in a standard optical fibre in the weak guidance regime, the spatial dependence of the $n^2(x,y;\omega_s)$ and $g_{a,b}(x,y,\Delta\omega)$ can be ignored since material interfaces are usually located at positions where

the fields have small intensity value, and thus these terms can be taken outside the integral in Eq. (28). Also in the weak guidance regime the modes are purely transverse thus the x-polarised and y-polarised modes are completely orthogonal (i.e. $\mathbf{e}_{sx}^* \cdot \mathbf{e}_{py} = 0$). Hence any interference terms between x and y polarised modes will have zero isotropic Raman gain. However contributions coming from the anisotropic component of the Raman gain can occur as we shall discuss later.

Emerging waveguides are interesting since the nonlinear susceptibility can have strong spatial dependence where the electric fields are at high intensity and as well x and y polarised modes can have significant overlap with each other due to their non-transverse nature [1]. This is quite fascinating as it leads to a new contribution to Raman gain not evident in previous analysis.

From here on we shall only explicitly show the contributions of the terms that do not require any phase matching i.e. $\beta_{p\eta} - \beta_{p\sigma} + \beta_{s\xi} - \beta_{s\mu} = 0$ for any arbitrary optical waveguide. This contracts the summation of modes to $\sigma = \eta$ and $\xi = \mu$. For $\sigma \neq \eta$ and/or $\xi \neq \mu$, the phase term $\beta_{p\eta} - \beta_{p\sigma} + \beta_{s\xi} - \beta_{s\mu}$ in general will be non-zero and typically very large. Thus the beat length of these interactions will be of the order of μm, thus will not contribute to any physically observed Raman effects within typical waveguides. It is however, possible to phase match these modes such that $\beta_{p\eta} - \beta_{p\sigma} + \beta_{s\xi} - \beta_{s\mu} = 0$ even for $\sigma \neq \eta$ and/or $\xi \neq \mu$, by correct tailoring of the modes of the MOF such that these phase terms cancel [37, 38].

$$
\begin{aligned}
\frac{\partial a_{s\mu}(z,t)}{\partial z} = {} & \hat{D} a_{s\mu} + \frac{g_{\mu\mu}}{2} \left[1 + \frac{i}{\omega_s} \frac{\partial}{\partial t} \right] |a_{p\mu}|^2 a_{s\mu} \\
& + \sum_{\eta \neq \mu} \frac{g_{\mu\eta}}{2} \left[1 + \frac{i}{\omega_s} \frac{\partial}{\partial t} \right] |a_{p\eta}|^2 a_{s\mu} \\
& + phase\,terms.
\end{aligned}
\tag{29}
$$

Where $g_{\mu\eta}(m^{-1}W^{-1})$ is the modal Raman gain experienced by the μth Stokes mode due to the presence of the ηth pump mode, which is now defined as:

$$
g_{\mu\eta} = \frac{\varepsilon_0^2 c^2}{4 N_{p\eta} N_{s\mu}} \int g_a n^2 \left| \mathbf{e}_{p\eta} \cdot \mathbf{e}_{s\mu}^* \right|^2 + g_b n^2 \left(\left| \mathbf{e}_{p\eta} \cdot \mathbf{e}_{s\mu} \right|^2 + \left| \mathbf{e}_{p\eta} \right|^2 \left| \mathbf{e}_{s\mu} \right|^2 \right) dA.
\tag{30}
$$

The modal Raman gain has now become a normalised weighted integral of the spatially dependent, bulk Raman gain coefficients, and refractive index profiles of the MOF, with the pump and Stokes fields. The VNSE can be rewritten in similar notation to the SM where we now define $\bar{g}_R$ as the effective Raman gain coefficient with respect to the intensity of fields inside the fiber and redefine the effective area to be $\bar{A}_{eff}$ where:

$$
g = \frac{\bar{g}_R}{\bar{A}_{eff}},
\tag{31}
$$

$$
\bar{A}_{eff} = \frac{\left(\int \mathbf{e}_{p\eta}^* \times \mathbf{h}_{p\eta} \cdot \hat{z} dA \right) \left(\int \mathbf{e}_{s\mu}^* \times \mathbf{h}_{s\mu} \cdot \hat{z} dA \right)}{\int \left(\mathbf{e}_{p\eta}^* \times \mathbf{h}_{p\eta} \cdot \hat{z} \right) \left(\mathbf{e}_{s\mu}^* \times \mathbf{h}_{s\mu} \cdot \hat{z} \right) dA},
\tag{32}
$$

$$
\bar{g}_R = \frac{\varepsilon_0^2 c^2 \int g_a n^2 \left| \mathbf{e}_{p\eta} \cdot \mathbf{e}_{s\mu}^* \right|^2 + g_b n^2 \left(\left| \mathbf{e}_{p\eta} \cdot \mathbf{e}_{s\mu} \right|^2 + \left| \mathbf{e}_{p\eta} \right|^2 \left| \mathbf{e}_{s\mu} \right|^2 \right) dA}{\int \left(\mathbf{e}_{p\eta}^* \times \mathbf{h}_{p\eta} \cdot \hat{z} \right) \left(\mathbf{e}_{s\mu}^* \times \mathbf{h}_{s\mu} \cdot \hat{z} \right) dA}.
\tag{33}
$$

The definition of the effective area in Eq. (32) is rather different to that in the SM which defines the effective area purely by the scalar transverse electric field distribution which is

assumed to be equal at both the pump and Stokes wavelengths. However, it can be shown that Eq. (32) reduces to the standard definition of the effective mode area [23] in the limit of weak guidance, as discussed in further detail in Section 3.

To understand the physical meaning of the effective area defined by Eq. (32) we shall discuss the simpler case where there is only one frequency (i.e. $p = s$) and one mode under consideration (i.e. $\eta = \mu$). Under these simplifications Eq. (32) becomes:

$$\bar{A}_{eff} = \frac{\left| \int (\mathbf{e}_\mu \times \mathbf{h}_\mu \cdot \hat{z}) dA \right|^2}{\int \left| (\mathbf{e}_\mu \times \mathbf{h}_\mu \cdot \hat{z}) \right|^2 dA}. \tag{34}$$

Eq. (34) is the definition of the effective area used in [1]. The physical interpretation of this form of the effective area is easier to identify as: the area of power flow of the μth eigenmode along the z-direction.

Here, we consider SRS at two different frequencies (p, s) and possibly between different modes. Thus the definition of the effective area given by Eq. (32), is an "average" of the areas of power flow along the z-direction of the μth pump mode and η^{th} Stokes mode.

The advantages in defining the modal Raman gain as in Eq. (31) is that it allows analysis to be separated into the linear properties of the optical waveguide that define $\bar{A}_{eff}$ and the nonlinear properties that are determined by $g_{a,b}(x, y)$. If one assumes that the anisotropic component of the Raman susceptibility is negligible within all materials of the optical waveguide, then $f_b = 0$ and $f_R = f_a$, and the analysis further simplifies to:

$$g = \frac{\varepsilon_0^2 c^2}{4N_{p\eta}N_{s\mu}} \int g_R n^2 \left| \mathbf{e}_{p\eta} \cdot \mathbf{e}_{s\mu}^* \right|^2 dA, \tag{35}$$

$$\bar{g}_R = \frac{\varepsilon_0^2 c^2 \int g_R n^2 \left| \mathbf{e}_{p\eta} \cdot \mathbf{e}_{s\mu}^* \right|^2 dA}{\int \left(\mathbf{e}_{p\eta}^* \times \mathbf{h}_{p\eta} \cdot \hat{z} \right) \left(\mathbf{e}_{s\mu}^* \times \mathbf{h}_{s\mu} \cdot \hat{z} \right) dA}.$$

The full form of the nonlinear pulse propagation Eq. as given by Eq. (28), is quite complicated and one must analyse the combination of propagation constants to see if the phase can be matched. For example in a single mode non-birefringent fiber then $\beta_{p\eta} - \beta_{p\sigma} = 0$ where η and σ are the x and y polarised modes respectively. In a standard optical fiber in the weak guidance regime, these modes have negligible overlap since the z-component of the electric field vector is negligible, but in the strong guidance regime where the z-component of the electric field vector becomes significant, the overlap can become significant. One may also need to consider the possibility of phase matching of higher order modes with lower order modes, forward and backward propagating modes for both the pump and Stokes fields.

Having developed the VNSE and formulated new definitions of the effective area and modal Raman gain for SRS we shall now investigate how these new formulations compare to the SM in Section 3. We shall explore which regimes show large differences between the two models and discuss the physical effects that cause these differences.

3. Significance of VNSE

The definition of the modal Raman gain by the VNSE now contains the contributions from the z-component of the electric field vector, which is neglected in the SM. Recent analysis [1, 25] has shown that the z-component of the electric field vector (E_z) can become significant in the presence of subwavelength features with high refractive index contrast. In [25] it was shown that for silicon wires at subwavlength dimensions, the fundamental quasi-TE mode can have longitudinal field amplitudes as high as 97% of the transverse field amplitudes.

It was shown in [1] for a high refractive index nanowire, as the size of the core decreases to subwavelength dimensions, the E_z fields have large magnitude and are confined more tightly to the nanowire. These features of the E_z fields makes these highly subwavelength core sized nanowires more desirable than previously considered with the SM that only considers the transverse fields.

To show the significance of this effect on Raman gain, we numerically model the effective area, $\bar{g}_R$ and $g(m^{-1}W^{-1})$ of a chalcogenide nanowire for a range of core diameters to observe in which regimes differences between the VNSE and SM can be significant. Here we take the refractive index of chalcogenide to be 2.4 [39]. We assume that due to the amorphous nature of chalcogenide glass, the bulk Raman gain coefficient is isotropic at the peak of the gain spectrum as found for silica glass [23, 36]. Also the pump and Stokes fields are co-polarised in all cases, except for VNSE ORTH in Fig. 2 where the pump and Stokes fields are taken to be orthogonally polarised. The pump wavelength is set to 1550 nm and here we consider only one value of the Raman gain spectrum, i.e. the peak which is located at 230 cm^{-1} [40] and corresponds to a Stokes wavelength of 1608 nm. At this Raman shift $g_R = 5.1 \times 10^{-11}$ mW^{-1} [40].

In Fig. 1 on the left we plot the effective area of a chalcogenide nanowire for a range of core diameters using the VNSE (red) as defined by Eq. (32), and using the SM [23] (blue). For large core diameters the two models become equivalent, which is where the modal field distributions have very small E_z fields, and thus the scalar approximation of the fields used by the SM is valid. However, at subwavelength core diameters, the VNSE predicts smaller effective areas with a minumum of 0.233 μm^2 than the SM with a minimum of 0.36 μm^2.

Thus we note that the energy within the mode can be confined more tightly than the transverse electric field distribution at nanowire dimensions located near the minimum effective area. This can be attributed to the z-component of the electric field vector as shown in [1], that the z-component of the Poynting vector is dependant on the e_z fields by:

$$S_z \propto \beta \left| \mathbf{e}_t \right|^2 - i\mathbf{e}_t \cdot \nabla_t e_z^*.$$

Thus when e_z becomes significant it can contribute to the effective area. As discussed in [1], the e_z fields maintain tighter confinement than the transverse electric fields for subwavelength core dimensions. Thus the e_z fields help to keep the mode tightly confined to the nanowire, further reducing the effective area.
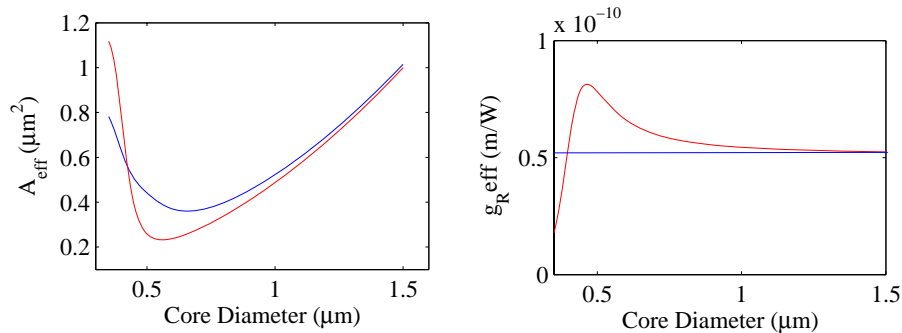

Fig. 1. Left: Effective area of a chalcogenide nanowire versus core diameter, using the VNLSE (Red) and SM (Blue). Right: Effective Raman gain coefficient of a chalcogenide nanowire versus core diameter using VNLSE (Red) and the bulk Raman gain coefficient is shown in blue.

On the right in Fig. 1 we plot the effective Raman gain coefficient of a chalcogenide nanowire

for a range of core diameters with the VNSE in red and bulk Raman gain coefficient in blue which is $g_R = 5.1 \times 10^{-11} \ mW^{-1}$. For large core diameters the effective Raman gain coefficient is approximately equal to the bulk Raman gain coefficient. As the size of the core decreases, the effective Raman gain coefficient rises above the bulk Raman gain coefficient, showing that the contributions from the e_z fields can create significant enhancement to the effective Raman gain coefficient. For even smaller core diameters the effective Raman gain coefficient decreases sharply from the peak. This occurs because the fields start to spread out into the air, decreasing the overlap of the fields with the Raman-active core.

We have seen that the z-component of the electric field vector can contribute significantly to reducing the effective area and enhancing the effective Raman gain coefficient at subwavelength core diameters. These two effects both increase the modal Raman gain. In Fig. 2 we calculate the modal Raman gain of the pump and Stokes fundamental modes of a chalcogenide nanowire for varying core diameter. In red we use the VNSE given by Eq. (35), in blue the SM given by Eq. (1), and in green the ASM used in [26]. Again, the pump wavelength is 1550 nm and the Stokes wavelength is 1608 nm.
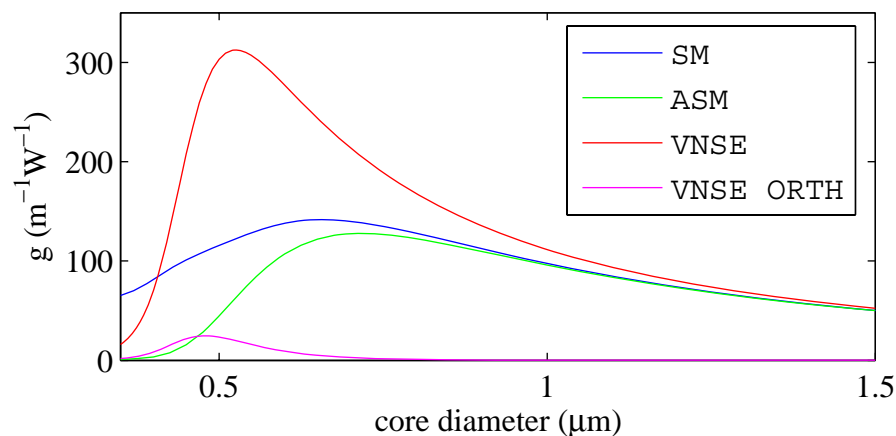

Fig. 2. Modal Raman gain of a Chalcogenide nanowire for varying core diameter. SM in blue, VNSE in red, ASM in green and VNSE ORTH in Pink. Pump wavelength 1550 nm, Stokes wavelength at 1608 nm.

We observe the convergence of the VNSE, SM, and ASM for core sizes of the order of the wavelength and larger. In this regime both pump and Stokes fields have high overlap, are contained completely within the core, and have negligible E_z components. However, for subwavelength core sizes, significant differences can be seen between the 3 models with a factor of over 2.5 observed between the VNSE and SM for a core diameter of 0.5 μm. Both the VNSE and ASM show a sharp decrease in modal Raman gain for core sizes smaller than 0.5 μm, which is due to the increase in effective area as well as decrease in overlap with the Raman active core as seen above in Fig. 1.

The modal Raman gain for orthogonally polarised pump and Stokes fields is plotted in pink in Fig. 2. In the regime of weak guidance (where the core size is relatively large) this contribution to Raman gain is negligible as assumed in [23], since the z-component of the fields approach zero and hence $\mathbf{e}_{px} \cdot \mathbf{e}_{sy} = 0$. However, at the subwavelength core sizes around 0.5 μm, the z-component of the fields can no longer be considered zero and hence $\mathbf{e}_{px} \cdot \mathbf{e}_{sy} \neq 0$ as discussed in Section 2. Thus the orthogonally polarised pump and Stokes fields will make a non-zero

contributions to Eq. (35), to the modal Raman gain. This contribution to the modal Raman gain can be as large as 10% of the modal Raman gain due to the co-polarised Stokes and pump fields for the same core diameter.

4. Tailoring the Raman Gain

Changing of the shape of the Raman gain spectrum can be very useful for applications such as telecommunications, where gain flattening techniques are applied to obtain an ultra-flat gain spectrum. Typical approaches to gain flattening of a Raman amplifier include using multiple pump sources [41, 42], designing the losses of the optical fiber [43], tailoring of the composition of the glass [44], etc. However, to the best of our knowledge, no reported techniques attempt to flatten the modal Raman gain spectrum by exploiting the wavelength dependence of the confinement of the fields to the optical fiber. The modal field distributions and the optical characteristics of a MOF can be tailored via modifying the complex fiber geometry, choice of the host glass material, as well as post fabrication processes such as filling the MOF with gases, liquids and atomic vapour. Thus MOFs offer flexibility for engineering the modal Raman gain to achieve gain enhancement, gain suppression or even change in the shape of the modal Raman gain spectrum.

Section 3 demonstrated the importance of considering the contributions from the z-component of the electric field vector. The VNSE also deviates from the SM in two other significant ways. The bulk Raman gain coefficient and refractive index of the optical waveguide in general are spatially dependent, and the pump and Stokes fields have different modal field distributions depending on the operating wavelength. These attributes suggest that the wavelength dependence of the Stokes modal field distributions $\mathbf{e}_{s\mu}$ will create a wavelength-dependent overlap of the Stokes fields with both the pump fields and the Raman active materials. Therefore, the shape of the modal Raman gain spectrum will not only depend on the bulk Raman gain coefficient spectrum, $g_R(\Delta\omega)$, but also the wavelength dependence of the waveguide's modal field distributions over the entire Raman spectrum. In contrast, the SM assumes that the effective area to be constant over the Raman spectrum and hence the shape of the modal Raman gain to be governed entirely by the bulk Raman gain coefficient. In [1] it was observed that at these subwavelength dimensions optical nanowires have strong wavelength dependence on the confinement of the modal fields to the core. Here we explore the use of this effect to tailor the shape of the modal Raman gain spectrum and investigate its use for gain flattening in Raman amplifiers.

Tellurite glass has a broad bandwidth bulk Raman gain coefficient [44-47], but requires significant gain flattening to be used as a Raman amplifier [46]. Fig. 2a shows an approximation of the tellurite bulk Raman gain spectrum based upon that in [45] using a super-Gaussian for the peak at 10 THz and a gaussian at 22 THz. The exact magnitude and shape of the bulk Raman gain spectra depends on the composition of the tellurite glass [44, 45]. As in [45] the bulk Raman gain coefficient spectrum contains a double peaked Raman gain spectrum. For simplicity we have simplified the gain spectrum using two Gaussian peaks. If we define the height of the peak at 22 THz divided by the height of the peak at 10 THz as R, then R = 2.0 for the bulk Raman gain coefficient. The value of R for the modal Raman gain is dependent on the design of the tellurite MOF. As discussed previously, in the regime of weak guidance, the effective area of the optical fiber is assumed to be constant over the Raman spectrum. This is shown in Fig. 3(b) in blue where the modal Raman gain spectrum for a tellurite nanowire with a core diameter 1.5 μm is shown. At this core size, both pump and Stokes fields are confined tightly to the Raman active core over all the Stokes wavelengths within the spectrum and the shape of the modal Raman gain looks identical to that of the bulk Raman gain coefficient with $R \approx 2.0$.
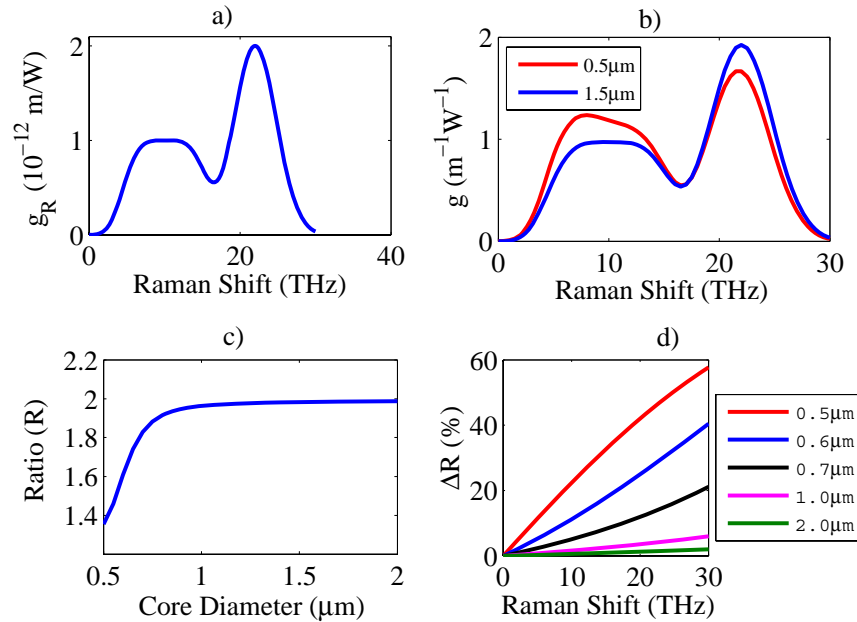
Fig. 3. a) Approximation of the bulk Raman gain coefficient spectrum of tellurite glass. b) Modal Raman gain spectrum of a tellurite nanowire for 1.5μm core diameter (cyan) and 0.5μm core diameter (red) calculated with the VNSE. c) Ratio (R) of the two peaks for varying core diameter. d) Plot of the amount of decrease in modal Raman gain due to finite overlap of the Stokes fields with the pump fields and the Raman active core.

However, if one considers a tellurite nanowire at the subwavelength core diameter of 0.5 μm as shown in Fig. 3(b) in red, a significant change in the shape of the modal Raman gain spectrum is observed with a decrease of the ratio of the peaks to $R = 1.35$. At this highly subwavelength core diameter, as we increase the Stokes wavelength, the Stokes modal field distributions further spread out from the core into the air, increasing the effective area as well as decreasing the overlap of the Stokes fields with both the Raman active core and pump modal field distribution. The resultant effect at this core diameter is a decrease in the confinement of the Stokes modal field distributions for increasing Raman shift (longer wavelength). The resultant modal Raman gain spectrum is a significantly flattened gain spectrum making this optical fiber more suitable in a Raman amplifier system.

To see how this flattening effect varies with core diameter, in Fig. 3(c) we plot R for varying core diameter of the optical nanowire. For larger core diameters R is close to 2.0 showing the convergence of the modal Raman gain to the SM in the regime of weak guidance. As the core diameter decreases to subwavelength dimensions, R reduces rapidly as the Stokes fields start to diverge out into the air. In order to observe the strength of this flattening effect across the spectrum, in Fig. 3(d) we plot ΔR, the amount of decrease in the modal Raman gain relative to the bulk Raman gain spectrum for a number of core diameters. As expected, the larger Raman shifts are affected more by this effect and these effects become more significant as we decrease the core size to subwavelength dimensions. Decreases in the modal Raman gain of up to nearly 60% are observed demonstrating the importance of considering these effects in the regime of strong guidance.

We have demonstrated the potential for significant alteration to the shape of the Raman gain spectrum through the diameter of a nanowire. However, the analysis here in an optical nanowire

has just only one free parameter to tailor the tellurite modal Raman gain spectrum, i.e. the core size of the nanowire. However, microstructured optical fibers have an arbitrary number of free parameters, such as the use of holes and inclusions of arbitrary shape and size within the MOF. Thus MOFs have more potential to further tailor the modal Raman gain by engineering the fiber geometry to achieve greater flattening, which is yet to be explored.

5. Conclusion and Discussion

The new frontier of optical waveguides containing subwavelength features, high refractive index contrast and complex structure lead to a regime of strong guidance. The standard models for describing nonlinear effects such as Kerr nonlinearity and stimulated Raman scattering are based upon weakly guiding optical waveguides, hence these standard models fail to accurately predict the modal Raman gain in this strong guidance regime. Here, we have followed on from the investigation in [1], and have developed a vectorial-based nonlinear Schrodinger Eq. (VNSE) for stimulated Raman scattering for accurate modeling in the strong guidance regime.

The VNSE in its most general form can model pulse propagation due to dispersion and SRS, for pulses longer and shorter than the Raman response time. However, we have assumed that the pump and Stokes fields have no spectral overlap, and that any dispersion in the Raman susceptibility tensor is contained within the Raman response function.

The VNSE takes into consideration the full vectorial form of the vector fields with the Raman susceptbility tensor and we have shown for silica MOFs that this leads to a different definition to the modal Raman gain than in standard models. We have numerically calculated the modal Raman gain with the VNSE to be over a factor of 2.5 larger than that calculated with the SM in soft glass optical nanowires. This observed increase in modal Raman gain is due to the contributions from the E_z fields, that in this regime of strong guidance, have large magnitude and tight confinement to the Raman active core. This increase in the modal Raman gain at subwavelength dimensions is expected have a great impact on creating highly efficient Raman devices.

Using a basis set of modes to describe the evolution of the pump and Stokes fields, has allowed the derivation of extra terms not considered in previous models [23, 27]. One implication of these extra terms is that unlike other models, a mode of the optical waveguide that initially has zero amplitude at the start of the waveguide can have non-zero amplitude under evolution due to the presence of other modes. Here we have not attempted to investigate the full potential of the VNSE, as we have only considered here the modal Raman gain between two fundamental modes. Future work is required to fully investigate the VNSE including pulse propagation simulations including bound and leaky modes, and investigating both the terms that are automatically phase matched and those that require phase matching. However, as discussed in Section 2, as we have not considered here the continuous set of space wave radiation modes, our basis set is not strictly complete. The impact of this on the accuracy of modelling pulse propagation simulations may need to be considered in certain regimes.

We have also observed in the strong guidance regime that significant modifications to the shape of the modal Raman gain spectrum can be achieved. Through engineering of the size of an optical nanowire in this strong guidance regime the ability to achieve flattening of a Raman gain spectrum was observed. However, the full potential of this technique has not been investigated by implementing further complex fiber geometry which may lead to further improvements in gain tailoring.